Random Forest Regression of Charge Balancing Data: A State of Health Estimation Method for Electric Vehicle Batteries

Alexander Lamprecht[1], Moritz Riesterer[1], Sebastian Steinhorst[2]
[1]TUMCREATE, Singapore, alexander.lamprecht@tum-create.edu.sg
[2]Technical University of Munich, Germany

***Abstract*—Recently, Electric Vehicles (EVs) are becoming more widespread. However, their mass adoption is hindered by the limited capacity of their Energy Storage System (ESS). Nowadays mainly Lithium-ion (Li-ion) technology is used for mobile applications, however, their energy density and cost put a hard limit on the maximum size of viable EV battery packs. Therefore, it is crucial to use existing technologies as effective as possible. To efficiently use a battery pack over its entire lifetime, the State of Health (SoH) of the cells needs to be taken into account. In this paper, we propose a novel SoH estimation method, based on the battery pack's behavior during Active Charge Balancing (ACB). From this behavior we are deriving a metric and show that it strongly correlates with the SoH. We use this metric, together with other cell parameters, to train a Random Forest (RF) regression estimator. To gather the training data, we implemented a modular simulation framework, that is able to reproduce the charging and discharging cycles, the charge balancing processes, as well as the aging behavior of battery packs over their entire lifetime. Besides showing a strong correlation between balancing behavior and SoH, we are able to estimate the cells' SoH with an accuracy of 1.94 % for the capacity and 4.28 % for the resistance, respectively. Our capacity SoH estimation outperforms state-of-the-art machine learning approaches, while we are among very few to even provide an estimate for the resistance with a high accuracy.**

I. Introduction and Related Work

In an era of climate change and a global shift to electrification in most aspects of society, sustainable Energy Storage System (ESS) play an increasingly important role. In most situations where ESS are used, it is of crucial importance to reliably estimate the remaining available energy.

Typical use cases are range estimation in Electric Vehicles (EVs) or PMDs as well as optimizing utilization in stationary storage systems. Most modern mobile ESS use Lithium-ion (Li-ion) battery technology, because of the high energy and power density. In Li-ion battery cells the remaining available energy level is indicated by the State of Charge (SoC). However, precise SoC estimation is challenging, as it is highly nonlinear and dependent on multiple variables, such as voltage, discharge rate, temperature and aging status. Particularly the last parameter has a significant influence on a given cell's performance in terms of power and capacity. It, therefore, is of central importance to estimate the aging status, which is typically represented by the SoH. To be able to reliably estimate a cell's SoC over its lifetime it is, therefore, necessary to also know about the cell's SoH. Accurate SoH estimation, however, proves difficult. Many different methods have been discussed in literature, such as extended Kalman Filter, enhanced Coulomb Counting, Electro Impedance Spectroscopy or even complex impedance analysis via Grey-Markov Chain

This work was financially supported in part by the Singapore National Research Foundation under its Campus for Research Excellence And Technological Enterprise (CREATE) programme. With the support of the Technische Universität München - Institute for Advanced Study, funded by the German Excellence Initiative and the European Union Seventh Framework Programme under grant agreement n° 291763.

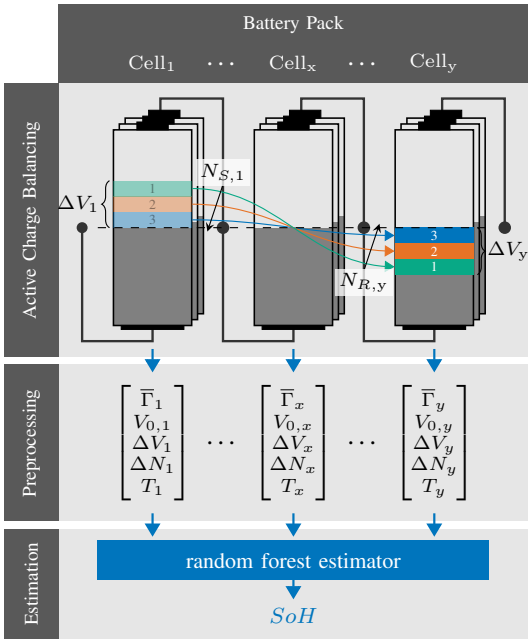

Fig. 1: Schematic representation of the process sequence of the simulation and analysis framework for a battery pack with y cells. Various parameters of the Active Charge Balancing (ACB) processes, such as the initial voltage at which a balancing process started V_0, the voltage difference caused by the balancing process ΔV, the discrepancy between the number of steps as charge sender and as receiver ΔN, the temperature T are recorded, collated and processed. This data is used to train a random forest estimator and allows accurate computation of the cell level State of Health (SoH) of the entire battery pack.

[1]–[3]. All these methods, however, require highly precise measurement of cell parameters, additional hardware or high computing power. Therefore, there has recently been a trend towards estimating the highly non-linear aging process with the help of Machine Learning (ML) such as Artificial Neural Networks (ANNs) [4]–[8].

In this paper we introduce a novel approach to estimate the SoH of Li-ion cells in large battery packs. For the first time the battery pack's behavior during ACB is utilized to conclude the SoH of each individual cell as shown in Fig. 1. We created a modular simulation framework (Fig. 4 on page 4), which is capable of replicating the aging and ACB behavior of battery packs over their entire lifetime and estimating the SoH via Random Forest (RF) regression.

Sections II&III give an overview of battery aging and ACB. The simulation framework is detailed in Section IV and the RF estimation method is explicated in Section V. Lastly, our results are presented and evaluated in Section VI, followed by a brief conclusion in Section VII.

Our specific contributions in this paper are:

- We implemented a comprehensive battery aging simulation framework, by extending the open source Cyber-Physical Co-Simulation Framework (CPCSF) from [9] with an empirical battery aging model based on [10] and a vehicle, drive cycle and climate model to apply different usage scenarios.
- We enhanced the CPCSF to clearly separate between physical battery model and a Battery Management System (BMS) model which allows the separation between the physical aging processes and calculations based on measurable data.
- We utilize a *random forest regressor*, trained by simulation results, to perform online SoH estimation on verification data.
- We are able to show that the SoH of the Li-ion cells can be deduced solely based on information drawn from the ACB (Section VI on page 4).
- The overall estimation accuracy of our method is 1.94 % for the capacity and 4.28 % for the internal resistance.

II. Aging of Li-Ion battery cells

While Li-ion technology currently is the industry standard for all sorts of non-stationary ESS applications, due to its superior power and energy density, it requires particular precautions during operation. If not used within distinct operation parameter limits, Li-ion technology can pose a significant safety risk. To ensure safe and reliable operation, every ESS based on Li-ion technology needs to be equipped with a BMS. Furthermore, Li-ion cells suffer from material degradation, conventionally referred to as aging.

Battery aging has two main causes. One is material degradation that happens based on time, commonly referred to as calendric aging. The second cause is cyclic aging, degradation resulting from usage of the cell [11].

The consequences of this material degradation are twofold. Firstly, a reduced energy storage capability due to a loss in usable capacity, and, secondly, a reduced power output due to increasing internal resistance.

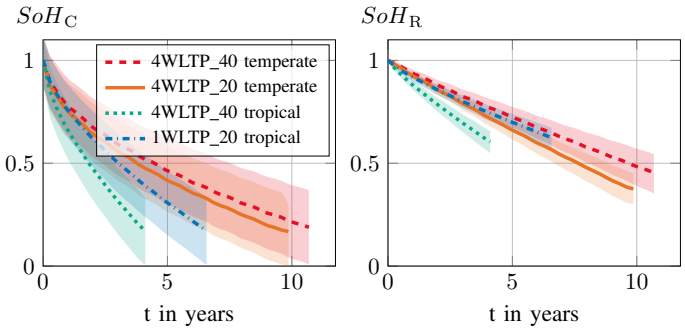

(a) SoH_C (b) SoH_R

Fig. 2: Decline of SoH_C and SoH_R of several battery packs over their life time for various usage patterns and climate scenarios.

To quantify these aging effects, the SoH is introduced. It is important to note that there is no standardized definition of the SoH and, therefore, different definitions can be found in literature [12]. In this paper we define the SoH as a weighted combination of two values, one for the loss in capacity (SoH_C) and one for the increase in internal resistance (SoH_R) with $SoH, SoH_\mathrm{C}, SoH_\mathrm{R} \in [0,1]$. A $SoH = 1$ represents nominal capacity or nominal internal resistance. For obvious practical reasons, End-of-life (EOL) criterions are chosen for the remaining capacity and the internal resistance, upon which the respective SoHs are defined to be 0. The criterion EoL_C is fulfilled if the remaining capacity C_m falls below 75 % of the nominal capacity C_n. The criterion EoL_R is fulfilled if the internal resistance $R_\mathrm{i,m}$ has doubled compared to the nominal internal resistance $R_\mathrm{i,n}$. SoH_C and SoH_R are therefore defined according to Equations 1 & 2.

$$SoH_\mathrm{C} = \left(\frac{C_\mathrm{m}}{C_\mathrm{n}} - EoL_\mathrm{C}\right) \cdot \frac{1}{1 - EoL_\mathrm{C}} \tag{1}$$

$$SoH_\mathrm{R} = \left(EoL_\mathrm{R} - \frac{R_\mathrm{i,m}}{R_\mathrm{i,n}}\right) \cdot \frac{1}{EoL_\mathrm{R} - 1} \tag{2}$$

The overall SoH of the battery pack is a combination of SoH_C and SoH_R.

The values for C_m and $R_\mathrm{i,m}$ are subject to aging, according to the empirical aging model in [10], and are updated every time the battery gets charged or discharged. Fig. 2 shows the decline in SoH_C and SoH_R over time for four battery packs with different usage scenarios until the EOL criterion is reached. The scenarios vary in usage pattern, charging frequency, Depth of Discharge (DoD) and ambient climate conditions. The aging calculation follows equations 3 and 4 and considers cyclic (β) as well as calendric (α) aging. These equations are taking the cell voltage V, the cell temperature T, the average voltage over one cycle $\overline{V}$ and the DoD DOD over one cycle into account, with $\alpha = f(V,T)$ and $\beta = f(\overline{V}, DOD)$. The resulting aging factors δ_C and δ_R represent the remaining capacity and internal resistance, respectively.

$$\delta_\mathrm{C} = 1 - \alpha_\mathrm{C} \cdot t^{0.75} - \beta_\mathrm{C} \cdot \sqrt{Q} \tag{3}$$

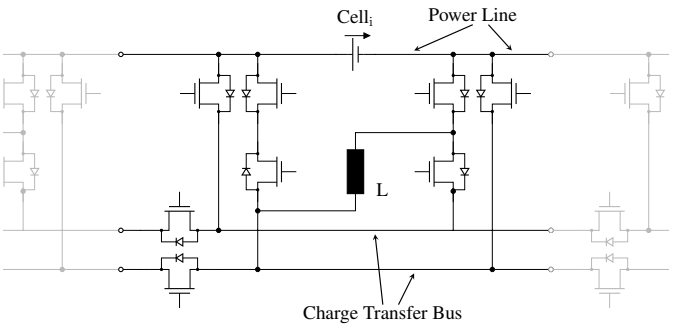

Fig. 3: The inductor based non-neighbor ACB architecture from [13] facilitates the charge transfers between cells.

$$\delta_{\mathrm{R}} = 1 + \alpha_{\mathrm{R}} \cdot t^{0.75} + \beta_{\mathrm{R}} \cdot Q \tag{4}$$

However, the factors α and β are characteristic to each individual cell and, therefore, replicate the heterogenous SoHs of physical cells. These SoHs variations, in turn, result in disparate SoCs. Not addressing these disparities leads to ever increasing charge imbalances between the cells, which diminish the overall usable pack capacity. It is therefore essential to periodically remove these imbalances via a process called charge balancing.

III. Charge Balancing in Large Battery Packs

Charge balancing is the process of altering remaining charge of a cell in a battery pack in order to equalize the SoC. While the current state-of-the-art solution of passive charge balancing equalizes the cells' SoC by dissipating excess energy over a resistor, ACB increases efficiency by transferring charge between cells [14]. Many different ACB architectures have been proposed in literature. All of which have in common that they are built around a temporary energy storage element. Typically this energy storage is either a capacitor, an inductor or a transformer. It has been shown that inductor based architectures offer the best trade-off between hardware complexity and efficiency gains [13]. In this paper therefore the architecture shown in Fig. 3 is utilized as the basis for the ACB. A single charge transfer, transferring a set amount of charge from one cell to another, is called a balancing step. One complete ACB process therefore consists of a sequence of balancing steps. It is controlled by the BMS via consensus algorithms that form a set of rules which are called strategies. These strategies decide during runtime which balancing step is to be executed next. They have a significant impact on the efficiency of the balancing process and have been discussed extensively in literature [9], [15]. In this paper only the proposed strategy from [15] will be applied, as it has proven to be highly efficient.

As the necessity for ACB is a consequence of aging, they are directly related. However, this relation has not yet been sufficiently examined in literature. The central idea behind this paper is, therefore, that the details of the balancing process directly correlate to aging.

IV. Simulation Framework

To investigate the correlation between the SoH and the ACB process, a simulation framework was developed. The framework is able to model a given battery pack over its entire lifetime and has three main functions.

Firstly it provides functionality for charging and discharging. Various charging regimes can be applied (Fast Charging/ Trickle Charging). As this paper focusses on automotive applications, a typical Constant Current, Constant Voltage (CCCV) charging method for Li-ion cells with 0.5 C was chosen. The discharging current is derived from the power demand of a vehicle model based on a Tesla Model S with a 85 kWh battery pack following the WLTP3 driving cycle, which is fed to the model in one second intervals. The vehicle model uses open source measurements for the ABC coefficients done by the EPA [16].

The second important component of the framework is an accurate aging model. To replicate the aging behavior of each individual cell, the empirical aging model from Section II is employed.

The third crucial component of the framework is the ACB functionality. This work is building on top of the CPCSF, presented in [9], as it provides many capabilities required for the desired simulation. Its realistic reproduction of the balancing process makes it perfectly suitable to verify our SoH estimation concept. Fig. 4 illustrates the structure of the simulation framework. It is implemented in Python, on top of the process-based discrete-event simulation tool SimPy.

The battery pack is modeled after a Tesla Model S battery pack with 18650 cells in 96S74P configuration and 85 kWh capacity [17]. To assess the accuracy of the SoH estimation method, every cell is split in two distinct models. One part to reproduce the physical cell behavior and aging effects, which we call the *physical model*, and a second part which contains the image of the given physical cell in the BMS, which we call the *Cell Management Unit (CMU) model*.

The physical model encompasses the battery cell itself characterized by its remaining maximum capacity C_{m}, charge level Q_{r}, internal resistance R_{i}, as well as temperature T and momentary current I. It furthermore contains the computed values for its $SoC = \frac{Q_{\mathrm{r}}}{C_{\mathrm{m}}}$ and its terminal voltage V. The value for R_{i} is dependent on the SoC and the temperature. The values for C_{m} and R_{i} are subject to aging according to the empirical aging model detailed in Section II and are updated after every discharge or charge cycle. Since this aging model is based on real physical measurements, it is reasonable to assume that the simulated cells behave realistically.

The CMU model contains the BMS, logic and communication components as well as a set of variables, imaging the current status of the physical cell model. The CMU model can interact with the physical model only by requesting the current voltage, current and temperature, which correlate to actual measurements of cell parameters.

Besides the sensing and measuring functionality and secondary data calculation, the CMU model also performs safety critical BMS functions like overvoltage and overcurrent protection and state monitoring.

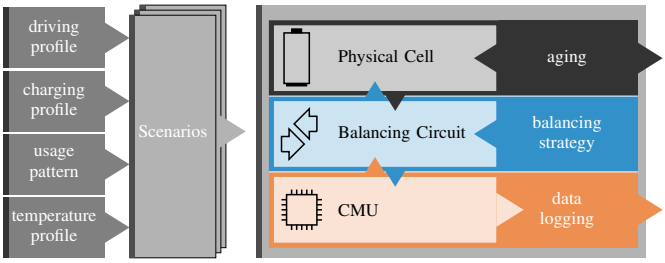

Fig. 4: Structure of the simulation framework. Scenarios are composed of driving and charging profiles, daily usage pattern, and temperature conditions and applied to the battery pack model.

The other central functionality of the model is the control of the ACB procedure. As described in Section III on the previous page, the ACB procedure is a sequence of individual balancing steps, each of which transfers a certain amount of charge between two cells. The sequence is controlled by strategies with the goal to converge all cells' SoCs to an equal value. Previously, while the overall efficiency in terms of time and losses of these strategies was paramount, the details of the individual balancing steps were neglected. The method proposed in this paper is based on exactly these balancing steps. Each step has a sender, a receiver and a frequency of occurrence. To record the individual balancing steps, the model includes a data logging module. Besides information about the balancing procedure from the CMU model, the logger also records aging data from the physical model.

V. SoH Estimation Method

To facilitate the SoH estimation, the previously recorded data from the simulation framework is used to train the estimator. The particular data values for a given cell with index i and a balancing process with index p are the initial voltage at which a balancing process started $V_{0,\mathrm{i,p}}$, the voltage difference caused by the balancing process $\Delta V_{\mathrm{i,p}}$, the discrepancy between the number of steps as sender and as receiver $\Delta N_{\mathrm{i,p}}$ and the temperature $T_{\mathrm{i,p}}$. We define $\gamma_{\mathrm{i,p}}$ as the quotient of the receiver/sender step discrepancy $\Delta N_{\mathrm{i,p}}$ and the voltage differential $\Delta V_{\mathrm{i,p}}$.

$$\gamma_{\mathrm{i,p}} = \frac{N_{\mathrm{s,i,p}} - N_{\mathrm{r,i,p}}}{\Delta V_{\mathrm{i,p}}} = \frac{\Delta N_{\mathrm{i,p}}}{\Delta V_{\mathrm{i,p}}} \tag{5}$$

Fig. 5 visualizes the correlation between $\gamma_{\mathrm{i,p}}$ and the SoH_{C}, exemplarily for one cell. Every entry of the scatterplot corresponds to data of one balancing process (Fig. 1). Even though the plot reveals a linear correlation between $\gamma_{\mathrm{i,p}}$ and SoH_{C}, it also shows the formation of two distinct bands, resulting in ambiguous SoH_{C} estimation values for a given $\gamma_{\mathrm{i,p}}$. Further analysis of $\gamma_{\mathrm{i,p}}$ established a strong impact of SoC_0^* on a shift in SoH. This shift was particularly well-defined for SoC_0^* values below 60 % and above 75 %. We figured, that it can be compensated by grouping several consecutive balancing processes together to one balancing cycle and weighted averaging their $\gamma_{\mathrm{i,p}}$ according to Equation 6, resulting in $\overline{\Gamma}_{\mathrm{i,p}}$. A balancing cycle is set to includes all balancing processes that happen between two charging process. Figuratively speaking, this operation bridges the gap between the bands in Fig 5 and, consequently improves estimation accuracy.

$$\begin{aligned}
\Gamma_{i,p} &= \left\{ \gamma_{i,p} \;\middle|\; \begin{array}{l} j \le p \le l \text{ with } j,p,l \in \mathbb{N} \\ SoC_{i,j-1} < 0.6 \wedge SoC_{i,j} > 0.75 \\ SoC_{i,l} < 0.6 \wedge SoC_{i,l+1} > 0.75 \\ min(p-j) \wedge min(l-p) \end{array} \right\} \\
&\gamma_{i,p} \in \Gamma_i \;\wedge\; \Gamma_{i,p} \subseteq \Gamma_i \\
\overline{\Gamma}_{i,p} &= \sum \beta_{i,p}\gamma_{i,p} \;\forall\, \gamma_{i,p} \in \Gamma_{i,p} \\
&\text{with } \beta_{i,p} = f(SoC_{i,p})
\end{aligned} \tag{6}$$

This resulting value $\overline{\Gamma}_{\mathrm{i,p}}$ is a remarkably accurate indicator for the SoH_{C} of a cell, as is shown in Section VI.

As illustrated in Fig. 1, $\overline{\Gamma}_{\mathrm{i,p}}$, together with the previously mentioned values, is used to train a Random Forest estimator. The RF estimator was chosen as it is a lightweight ensemble learning method that exhibits an acceptable trade off between regression analysis accuracy and computational complexity [18]. In future research more sophisticated methods, such as the Gradient Boosting Machine, could be applied, as they promise improved accuracy and performance [19]. The RF regression uses the open-source machine learning Python library Scikit-learn.

Training of the RF estimator was done with data from an array of scenarios, with variations in usage pattern, climate conditions and SoC limit below which charging is triggered. The usage pattern defines the the time a car is driven per day. It is varied in 1 h steps from 1 h to 4 h, during which the standardized WLTP3 driving cycle is repeated until the time is up or the battery pack is empty. After each day the battery pack is charged if the SoC falls below a threshold. This threshold is varied between 20 % and 40 % SoC. Lastly the climate conditions are varied to either apply a constant temperature (tropical climate) or a seasonally changing temperature (temperate climate).

For each scenario the entire lifetime of four battery packs with individual initial cell SoH distributions and aging factors are simulated. A random subset of data from each scenario and battery pack was picked for training (3 out of the 4 battery packs for 12 out of 16 scenarios; 56.25 %) and the remaining data was used for validation (1 out of the 4 battery packs for 12 out of 16 scenarios; 18.75 %) and testing (4 out of the 4 battery packs for 4 out of 16 scenarios; 25 %). For hyperparameter tuning of bootstrap, the number of trees and features for decision are validated using a 5-fold cross-validation on the training data. In an additional evaluation step using the validation data set we have found, that a tree depth of 17 provides the best performance level while the error remains unchanged. Increasing the tree depth results in ever increasing demand for memory and storage space.

VI. Results

In this section the results we obtained from our simulation are discussed. The simulation was conducted for battery packs with 96S74P configuration with 85 kWh as it is used in a Tesla's Model S. The aging behavior of four battery packs for each of 16 different scenarios were simulated until they

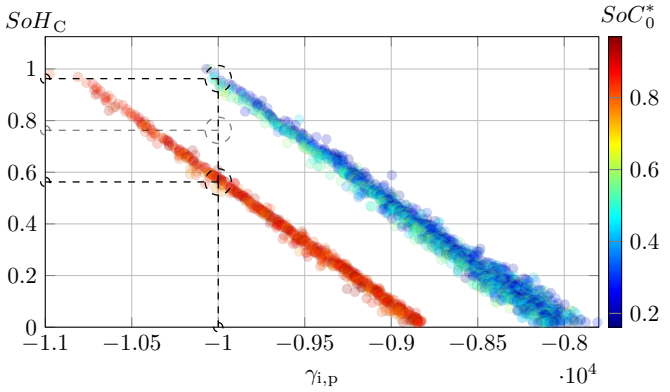

Fig. 5: Scatterplot of the SoH_C values over $\gamma_{i,p}$ for all balancing processes during the entire life time of one cell. The color gradient indicates the SoC at the beginning of each balancing process.

reached their EOL. Typical simulation runtime, for one battery pack, ranges from 50 h to 70 h depending on the aging rate. The resulting simulation data was used to train a RF regression estimator. Therefore, data from 12 of the 16 scenarios were used for the training process. Data from the remaining 4 scenarios, which has not been used to train the estimator, was used for testing. Fig. 6 visualizes the estimation results. On the left side the results for the SoH_C are displayed, and on the right side, the results for the SoH_R respectively. Fig. 6a showcases the SoH^* estimation results after each balancing process (scatter plot), overlaid with the actual SoH values (solid line) over the entire lifetime of two different battery packs. For each battery pack only the cells with the lowest (darker), respectively highest (lighter), SoH are displayed. These two battery packs exhibit different aging behavior and, therefore, life span, due to their usage scenarios. $Pack_1$ (blue) was cycled in a moderate climate with only 1 h of usage a day, resulting in >4000 days before reaching its EOL. $Pack_2$ (orange) on the other hand, was cycled in a tropical climate with higher average temperatures with intense usage and was regularly discharged to low SoC values, which reduces its life time to <2000 days. Both plots in Fig. 6a show the estimation accuracy of the RF estimator over the entire lifetime of the pack. The estimation accuracy for the SoH_R slightly worsens over time, resulting in a wider spread in the estimation values, while it stays almost constant for the SoH_C. It is important to note, that even though the battery cells showed vastly different aging behavior, depending on their usage scenario, the estimation algorithm performed well indiscriminately.

Fig. 6b displays the relative frequency histograms of the estimation errors AE_C and AE_R for all 4 testing scenarios with 4 battery packs each; over $2.5 \cdot 10^6$ data points in total. It, therefore, quantifies the estimation accuracy for all simulations, with a resulting Root Mean Square Error (RMSE) values for the capacity estimation of $RMSE_C$ = 1.94 % and for the resistance estimation of $RMSE_R$ = 4.3 %. These results come from data sets that have previously not been used for training and are therefore unknown to the algorithm. Furthermore, these results have been achieved based on data

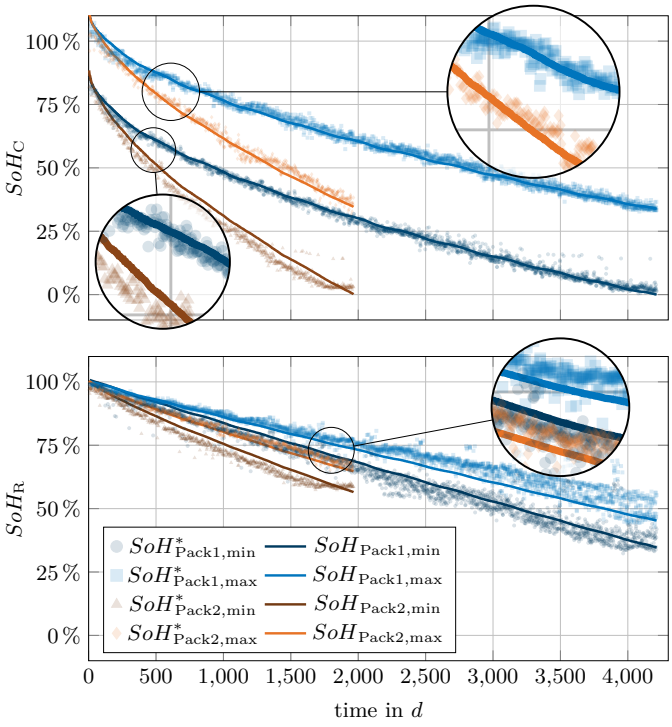

(a)

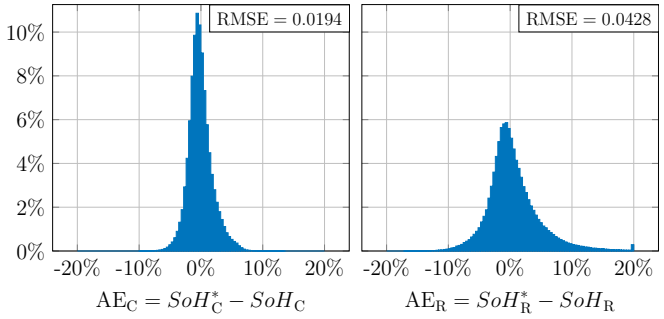

(b)

Fig. 6: Results of the SoH estimation.
(a) Plot of the measured (scatter plot) and estimated (solid line) SoH_C and SoH_R of two battery packs over their entire life time. The darker color plots represent the lowest SoH cell (min) and the lighter color plots represent the highest SoH cell (max) of each pack.
(b) Relative frequency histogram of the estimation error AE_C and AE_R for all balancing processes from 16 scenarios, each with four individual battery packs with 96S74P configuration. 2.5 million data points in total.

from scenarios different to those of the training data set, furthering their generality. We therefore expect, that similar results can be achieved with a different data set.

Table I compares our estimation accuracy with other ML based SoH estimation approaches found in literature. Where most other approaches are solely focusing on the SoH_C and neglect the SoH_R, our method gives a consistently accurate estimation for both values. Our approach clearly outperforms state-of-the-art machine learning approaches for the SoH_C,

TABLE I: Comparison of SoH estimation performances between this paper's method and other ML approaches found in literature.

source	ML type	$\mathrm{RMSE_C}$	$\mathrm{RMSE_R}$	notes
[4]	ANN	4.24 %*	N/A	-
[5]	RNN	8.28 %*	1.32 %	values converted from their Mean Squared Error definition
[6]	DNN	13.72 %*	N/A	no temperature variations considered
[7]	RF	2.52 %*	N/A	no temperature variations considered
[8]	RF	5.20 %*	N/A	-
this paper	RF	1.94 %	4.28 %	ref. Section V

* values are normalized to match this paper's SoH definition, incorporating the EOL criteria (Section II), to ensure comparability.

while we are among very few to even provide an estimate for the SoH_R with a high accuracy. Naturally for ML algorithms,

	SoH_C	SoH_R
$\overline{\Gamma}_{\mathrm{i,p}}$	0.9376	0.8425
$V_{0,\mathrm{i,p}}$	0.0171	0.0403
$\Delta V_{\mathrm{i,p}}$	0.0198	0.0267
$\Delta N_{\mathrm{i,p}}$	0.0230	0.0184
$T_{\mathrm{i,p}}$	0.0025	0.0721

TABLE II: Feature importance for the random forest estimator.

the different features of the input vector have varying degrees of impact on the outcome. Table II lists the feature importance of the input variables for the estimated SoH_C and SoH_R. The significance of $\overline{\Gamma}_{\mathrm{i,p}}$, particularly for the SoH_C estimation, with 93.8 % importance, becomes apparent.

VII. Conclusion

In this paper we propose a novel approach to estimating the SoH of cells in large battery packs with ACB by Random Forest regression of data from the charge balancing processes. Therefore, we implemented a modular simulation framework, that is able to reproduce the charging and discharging cycles, the charge balancing processes, as well as the aging behavior of battery packs over their entire lifetime. With simulation results from an array of scenarios, consisting of different drive cycles, usage patterns, and seasonal temperature profiles, we are able to train a RF regression model to do online SoH estimation. Not only did we show a strong correlation between balancing behavior and SoH, but we were also able to quantify this this correlation with an accuracy of 1.94 % for the capacity and 4.28 % for the resistance respectively. As typical BMSs in EV do not possess the necessary memory or computing capacity to execute the estimation, these calculations could either be performed remotely via a cloud service or via peripheral hardware. Since modern vehicles are equipped with sophisticated computing hardware to facilitate driver assisting tasks, such as NVIDIA DRIVE AGX, the estimation could be outsourced to these components when they are not in use. Future research could refine the estimation method by investigating the performance of other ML techniques, such as Boosted Regression Trees, as they promise improvements.

References

[1] C. Lin, A. Tang, and W. Wang, "A Review of SOH Estimation Methods in Lithium-ion Batteries for Electric Vehicle Applications," *Energy Procedia*, vol. 75, pp. 1920–1925, 2015.

[2] P. A. Topan, M. N. Ramadan, G. Fathoni, A. I. Cahyadi, and O. Wahyunggoro, "State of Charge (SOC) and State of Health (SOH) estimation on lithium polymer battery via Kalman filter," *Proceedings - 2016 2nd International Conference on Science and Technology-Computer, ICST 2016*, no. 2, pp. 93–96, 2017.

[3] D. I. Stroe and E. Schaltz, "SOH Estimation of LMO/NMC-based Electric Vehicle Lithium-Ion Batteries Using the Incremental Capacity Analysis Technique," *2018 IEEE Energy Conversion Congress and Exposition, ECCE 2018*, no. Ic, pp. 2720–2725, 2018.

[4] G. won You, S. Park, and D. Oh, "Real-time state-of-health estimation for electric vehicle batteries: A data-driven approach," *Applied Energy*, vol. 176, pp. 92–103, 2016.

[5] A. Eddahech, O. Briat, N. Bertrand, J. Y. Delétage, and J. M. Vinassa, "Behavior and state-of-health monitoring of Li-ion batteries using impedance spectroscopy and recurrent neural networks," *International Journal of Electrical Power and Energy Systems*, vol. 42, no. 1, pp. 487–494, 2012.

[6] P. Khumprom and N. Yodo, "A data-driven predictive prognostic model for lithium-ion batteries based on a deep learning algorithm," *Energies*, vol. 12, no. 4, 2019.

[7] Z. Chen, M. Sun, X. Shu, J. Shen, and R. Xiao, "On-board state of health estimation for lithium-ion batteries based on random forest," *Proceedings of the IEEE International Conference on Industrial Technology*, vol. 2018-February, pp. 1754–1759, 2018.

[8] Y. Li, C. Zou, M. Berecibar, E. Nanini-Maury, J. C. Chan, P. van den Bossche, J. Van Mierlo, and N. Omar, "Random forest regression for online capacity estimation of lithium-ion batteries," *Applied Energy*, vol. 232, no. February, pp. 197–210, 2018.

[9] S. Steinhorst, M. Kauer, A. Meeuw, S. Narayanaswamy, M. Lukasiewycz, and S. Chakraborty, "Cyber-physical co-simulation framework for smart cells in scalable battery packs," *ACM Transactions on Design Automation of Electronic Systems (TODAES)*, vol. 21, pp. 62:1–62:26, 5 2016.

[10] J. Schmalstieg, S. Käbitz, M. Ecker, and D. U. Sauer, "A holistic aging model for Li(NiMnCo)O2 based 18650 lithium-ion batteries," *Journal of Power Sources*, vol. 257, pp. 325–334, 2014.

[11] A. Barré, B. Deguilhem, S. Grolleau, M. Gérard, F. Suard, and D. Riu, "A review on lithium-ion battery ageing mechanisms and estimations for automotive applications," *Journal of Power Sources*, vol. 241, pp. 680–689, 2013.

[12] S. M. Rezvanizaniani, Z. Liu, Y. Chen, and J. Lee, "Review and recent advances in battery health monitoring and prognostics technologies for electric vehicle (EV) safety and mobility," *Journal of Power Sources*, vol. 256, pp. 110–124, 2014.

[13] M. Lukasiewycz, M. Kauer, and S. Steinhorst, "Synthesis of active cell balancing architectures for battery packs," *IEEE Transactions on Computer-Aided Design of Integrated Circuits and Systems (TCAD)*, vol. 35, no. 11, pp. 1876–1889, 2016.

[14] F. Baronti, R. Roncella, and R. Saletti, "Performance comparison of active balancing techniques for lithium-ion batteries," *Journal of Power Sources*, vol. 267, pp. 603 – 609, 2014.

[15] A. Lamprecht, M. Baumann, T. Massier, and S. Steinhorst, "Decentralized non-neighbor active charge balancing in large battery packs," in *2019 Design, Automation Test in Europe Conference Exhibition (DATE)*, pp. 432–437, March 2019.

[16] M. Ates and R. D. Matthews, "Coastdown coefficient analysis of heavy-duty vehicles and application to the examination of the effects of grade and other parameters on fuel consumption," in *SAE Technical Paper*, SAE International, 09 2012.

[17] M. Lelie, T. Braun, M. Knips, H. Nordmann, F. Ringbeck, H. Zappen, and D. Sauer, "Battery management system hardware concepts: An overview," *Applied Sciences*, vol. 8, p. 534, 03 2018.

[18] R. Couronné, P. Probst, and A.-L. Boulesteix, "Random forest versus logistic regression: a large-scale benchmark experiment," *BMC Bioinformatics*, vol. 19, p. 270, dec 2018.

[19] F. Chollet, *Deep Learning with Python*. Manning, Nov. 2017.